Universität Karlsruhe (TH)
Forschungsuniversität • gegründet 1825

Institut für Mechanik

Benchmark Computations of low and high order Shell Elements on adaptively generated FE Meshes

S. Kizio, K. Schweizerhof
Universität Karlsruhe, Institut für Mechanik

A.Düster, E. Rank
Technische Universität München, Lehrstuhl für Bauinformatik

Institut für Mechanik
Kaiserstr. 12, Geb. 20.30
76128 Karlsruhe
Tel.: +49 (0) 721/ 608-2071
Fax: +49 (0) 721/ 608-7990
E-Mail: ifm@uni-karlsruhe.de
www.ifm.uni-karlsruhe.de

Benchmark Computations of low and high order Shell Elements on adaptively generated FE Meshes

S. Kizio, K. Schweizerhof
Institut für Mechanik
Universität Karlsruhe

A. Düster, E. Rank
Lehrstuhl für Bauinformatik
Technische Universität München

Abstract

Low order shell and more recently so-called solid-shell elements are very popular in finite element computations of shell structures. Meshes for low order elements can easily be generated and due to the small bandwidth of the system matrix the solution effort is relatively low. In addition they are numerically very robust for nonlinear and large deformation problems. At a first look a major disadvantage is that many locking phenomena occur which however, can be reduced and often removed by various modifications. An often overlooked problem of low order elements is their reduced capacity to capture the geometry of curved shell structures and their deficiencies in non-regular meshes. Subject of this study is the comparison of different modifications of low order solid-shell elements by means of numerical examples using adaptively generated meshes including arbitrary shapes of the elements. A particular focus is on the comparison of low order elements with high order elements.

Zusammenfassung

Der vorliegende Beitrag befasst sich mit dem Vergleich von Volumen-Schalen-Elementen niedriger Ansatzordnung mit Finite-Element-Formulierungen hoher Ansatzordnung anhand eines numerischen Beispiels. Es werden bilineare und biquadratische Volumen-Schalen-Elemente mit verschiedenen Modifikationen zur Beseitigung von Versteifungseffekten sowie Volumenelemente mit isotropem und anisotropem Ansatz für das Verschiebungsfeld betrachtet. Um den Einfluss unregelmäßiger Elementgeometrien auf das Konvergenzverhalten zu untersuchen, werden die Netze für die Volumen-Schalen-Elemente mit uniformer sowie adaptiver Netzverfeinerung verschiedener Ausgangsdiskretisierungen generiert.

1 Introduction

Subject of this study is the comparison of different low order shell elements based on the solid-shell concept, e.g. [14–18], by means of numerical examples on adaptively generated meshes. As a reference the p-version of the finite element method [11, 24] is included.

A hierarchical mesh adaptation scheme is chosen here for the mesh generation since the use of transition elements between refined and non-refined regions of the spatial discretization automatically results in distorted element geometries which is mandatory for general element tests. In other studies, e.g. by Pitkäranta et al. [23] or Bathe et al. [2] distorted spatial discretizations are introduced artificially.

The adaptive refinement of meshes therefore seems to be an appropriate tool for the automatic generation of suitable spatial discretizations for tests of solid-shell elements.

2 Effects of hierarchical adaptive mesh refinement

As it is known from several publications concerning computations of shell problems, e.g. [2, 19, 22, 23] in shell analyses three types of deformation states have to be distinguished: a) dominant

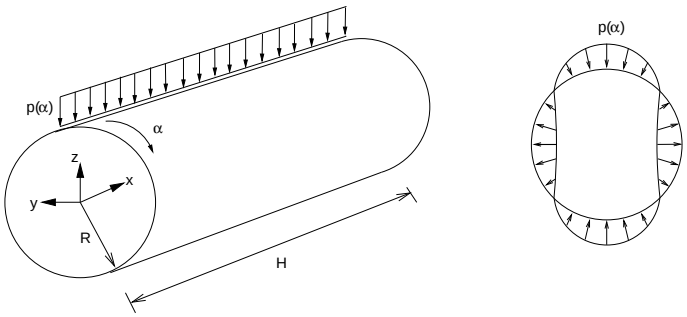

Fig. 1 Cylindrical shell under external pressure

membrane deformation states, b) bending dominated or inextensional deformation states and c) mixed deformation states where neither the membrane nor the bending part is dominant. The most critical deformation state for finite element computations using low order shell elements is the bending dominated case. Then the results are known to be very sensitive to mesh distortions. In contrast, low order shell elements even with fairly strong mesh distortions are well-suited for analyses of problems where the membrane energy is dominant.

The relevance of the above mentioned classification of deformation states as well as the influence of an adaptive refinement in the cases a) and b) shall be briefly discussed in the following considering an example introduced by Pitkäranta et al. in [23], see figure 1.

The cylindrical shell has the length $H = 2 \cdot R$ and consists of isotropic material with Young's modulus E and Poisson ratio ν. The shell is loaded by a normal pressure distribution on the outer surface which is constant in x-direction and varies angularly as:

$$p(\alpha) = p_0 \cdot cos2\alpha \tag{1}$$

The deformation state strongly depends on the boundary conditions at both ends of the shell structure. Fully clamped ends result in a dominant membrane deformation state (case a) with boundary layers in the vicinity of the ends. These boundary layers are always bending dominated. Free ends yield a dominant bending state (case b). Note, that the applied loading is self balancing and hence no boundary conditions are necessary to achieve equilibrium.

The problem is now computed using simple 4-noded bilinear shell elements with assumed natural shear strain interpolation (ANS4-element) [12, 13]. Due to the symmetry of the problem only one eighth of the shell is discretized. In both cases uniform and adaptive mesh refinement is performed starting with a coarse mesh consisting of 4x4 elements. The adaptive mesh refinement is based on the estimation of the error in the energy norm applying the SPR-concept of Zienkiewicz and Zhu [29, 30]. The applied refinement strategy is described in detail in [3, 25].

Figure 2 shows the evolution of the relative error for the mesh refinements in both cases. It can clearly be seen that the adaptive approach improves the solution behavior in case of the membrane dominated problem. However in case of the bending dominated problem the solution is strongly perturbed by the adaptive mesh refinement.

The improvement in case a) results dominantly from the fine discretization of the boundary layers, i.e. the resulting mesh is graded towards the ends of the shell. Furthermore mainly rectangular elements aligned to the curvature of the cylinder occur in the bending dominated

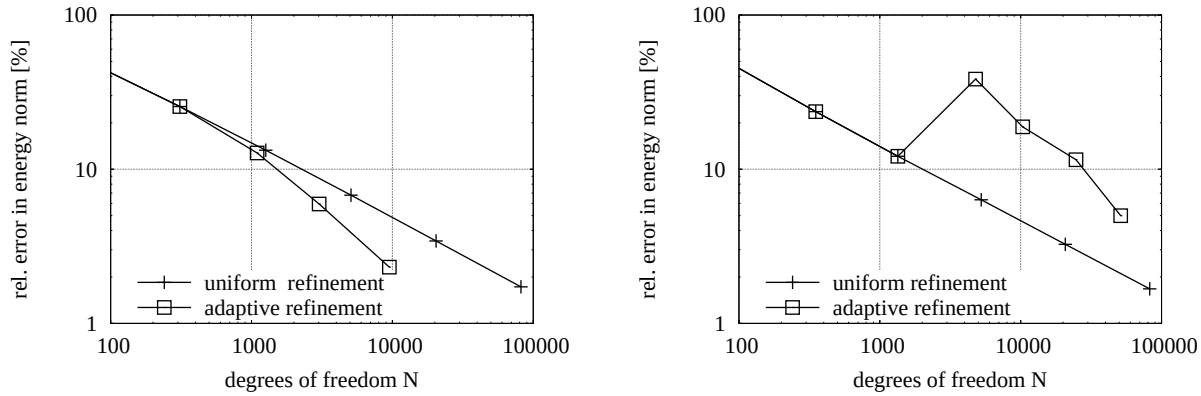

Fig. 2 Cylindrical shell under external pressure load, variation of boundary conditions at ends: Convergence diagrams (relative error in energy norm) for uniform and adaptive mesh refinement

boundary layer, see figure 3. Badly shaped elements mainly occur at the transition of the bending dominated boundary layer to the membrane dominated part of the shell.

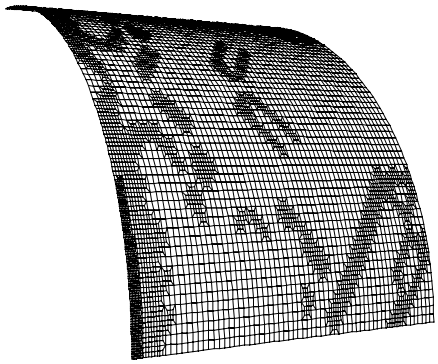

Fig. 3 Cylindrical shell: Spatial discretization in last adaptive refinement step case a) fully clamped ends. FE model 1/8 of structure with symmetry boundary conditions

The unfavorable effect of the adaptive scheme in the bending dominated case b) (free ends) results from the fact that the edges of the transition elements, which are now in regions with fairly strong bending, are not aligned with the generatrix of the shell which - as is known - strongly perturbes the performance of low order shell elements in bending dominated problems.

3 Benchmark study

In the following a benchmark problem is introduced to compare the effects of different modifications of low order elements and their performance in a bending dominated problem. The rest of the report is organized as follows: First the elements used in the study are presented in a brief manner. After the introduction of the bending dominated benchmark problem the results achieved with the different element types are compared.

3.1 Survey of elements used in the study

The elements used in the study are presented only in a very brief manner. For a more detailed discussion of the solid-shell elements we refer to [14, 15, 18]. Basically three approaches are used for removing the several locking phenomena, the enhanced assumed strain (EAS) approach by Simo and Rifai [26, 27], the assumed strain approach (ANS) (e.g. [12]) and the discrete strain gap method (DSG) [7].

3.1.1 Bilinear solid-shell elements

First solid-shell elements with bilinear interpolation in in-plane direction are discussed, i.e. the upper and lower shell surface are discretized each by four nodes. This involves bilinear interpolation of the geometry and of the displacements.

3.1.2 Modifications of transversal shear strains

Two approaches to remove transverse shear locking are presented here. The first is the assumed natural strain method (ANS) where the transverse shear strains are interpolated as proposed by Bathe and Dvorkin [12]:

$$\begin{aligned} E^{ANS}_{\xi\zeta}(\xi,\eta,\zeta) &= \frac{1}{2}[1-\eta]E_{\xi\zeta}(\xi=0,\eta=-1,\zeta)+\frac{1}{2}[1+\eta]E_{\xi\zeta}(\xi=0,\eta=+1,\zeta) \quad (2)\\ E^{ANS}_{\eta\zeta}(\xi,\eta,\zeta) &= \frac{1}{2}[1-\xi]E_{\eta\zeta}(\xi=-1,\eta=0,\zeta)+\frac{1}{2}[1+\xi]E_{\eta\zeta}(\xi=+1,\eta=0,\zeta) \end{aligned}$$

The second approach is the discrete strain gap method (DSG) introduced by Bletzinger et al. [5, 7] where the so-called strain gaps (which are integrals of the transversal shear) of all nodes are interpolated using the same Ansatz functions as for the displacements and geometry. Since these strain gaps are displacements, the modified transversal shear strain distribution is obtained by differentiation of the interpolated strain gaps. The modified strains then read:

$$\begin{aligned} E^{DSG}_{\eta\zeta}(\xi,\eta,\zeta) &= \sum_{m=1}^{n_{np}}\left[N^m_{,\zeta}\int_{\zeta_0}^{\zeta_m}\left(\sum_i^{n_{np}}N^i_{,\eta}\int_{\eta_0}^{\eta_i}E_{\eta\zeta}d\eta\right)d\zeta\right] \quad (3)\\ E^{DSG}_{\xi\zeta}(\xi,\eta,\zeta) &= \sum_{m=1}^{n_{np}}\left[N^m_{,\zeta}\int_{\zeta_0}^{\zeta_m}\left(\sum_i^{n_{np}}N^i_{,\xi}\int_{\eta_0}^{\eta_i}E_{\xi\zeta}d\xi\right)d\zeta\right] \end{aligned}$$

The DSG-method results in a direct modification of the displacement-strain operator $\mathbf{B}$ and is very efficient.

For elements with a constant determinant of the Jacobian of the isoparametric map the ANS and DSG approach yield identical stiffness matrices. Therefore the two approaches do not need to be compared in the numerical benchmark problem.

3.1.3 Modification of membrane strains

The modifications of the membrane strains are introduced to remove membrane locking. Here two approaches are discussed. The first approach is the enhancement of the in-plane strains with the enhanced assumed strain method (EAS) originally proposed by Simo and Rifai [26]:

$$\boldsymbol{E}_{ip}^{EAS} = \begin{pmatrix} E_{\xi\xi} \\ E_{\eta\eta} \\ 2E_{\xi\eta} \end{pmatrix} = \boldsymbol{E}_{ip}^{c} + \boldsymbol{M}\boldsymbol{\alpha} \tag{4}$$

The vector $\boldsymbol{E}_{ip}$ contains the in-plane Green-Lagrange strains, where $\boldsymbol{E}_{ip}^{c}$ are the strains compatible to the displacements. For brevity no further details on the construction of the enhanced strains are discussed here. For the proper incorporation of the method into the solid-shell concept and for the discussion of the different versions we refer to [14, 15, 18].

The second approach is the modification of the strains with the discrete strain gap method [7, 21]:

$$\begin{aligned} E_{\xi\xi}^{DSG} &= \sum_{i=1}^{n_{np}} N_{,\xi}^{i} \int_{\xi_0}^{\xi_i} E_{\xi\xi} d\xi \\ E_{\eta\eta}^{DSG} &= \sum_{i=1}^{n_{np}} N_{,\eta}^{i} \int_{\eta_0}^{\eta_i} E_{\eta\eta} d\eta \\ E_{\xi\eta}^{DSG} &= \sum_{m=1}^{n_{np}} \left[N_{,\eta}^{m} \int_{\eta_0}^{\eta_m} \left(\sum_{i}^{n_{np}} N_{,\xi}^{i} \int_{\xi_0}^{\xi_i} E_{\xi\eta} d\xi \right) d\eta \right] \end{aligned} \tag{5}$$

3.1.4 Thickness locking

Solid-shell elements suffer from thickness locking if a linear displacement assumption in thickness direction is used. The normal thickness strain $E_{\zeta\zeta}$ is then constant in thickness direction. However, since $E_{\zeta\zeta}$ is coupled with the in-plane normal strains $E_{\xi\xi}$ and $E_{\eta\eta}$ via the Poisson-ratio, $E_{\zeta\zeta}$ must be distributed linearly in thickness direction in order to capture bending dominated deformation states.

For all solid-shell elements used in the study thickness locking is removed by a linear enhancement of the thickness normal strains applying the EAS-method with 4 additional element parameters α_i, see [9, 10]:

$$E_{\zeta\zeta}^{EAS} = E_{\zeta\zeta}^{c} + \frac{1}{det\boldsymbol{J}} \zeta [1 \; \xi \; \eta \; \xi\eta] \begin{pmatrix} \alpha_1 \\ \alpha_2 \\ \alpha_3 \\ \alpha_4 \end{pmatrix} \tag{6}$$

Herein $det\boldsymbol{J}$ denotes the determinant of the Jacobian of the isoparametric map.

3.1.5 Curvature-thickness-locking

Curvature-thickness-locking is the artificial coupling of pure bending states with the normal thickness strains $E_{\zeta\zeta}$. This phenomenon occurs when the directors at the element edges - resp. the vector pointing from the lower to the upper node of the edge of the solid-shell element - are not perpendicular to the element midplane. This problem automatically arises in case of a regular discretization of a curved geometry when the directors should be perpendicular to the exact shell geometry. See for example the regular discretization of a cantilever curved shell shown in figure 4, where all directors point to the center of curvature O.

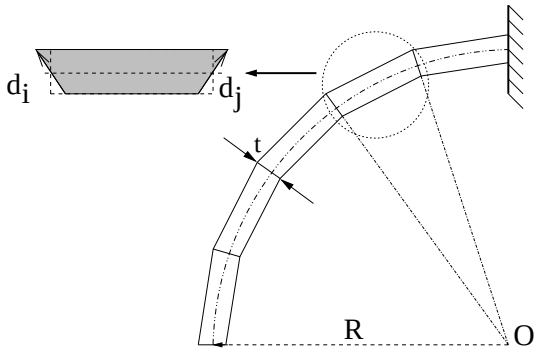

Fig. 4 Curvature-thickness-locking: Regular discretization of a curved cantilever shell

To avoid this locking behavior an assumed transverse normal strain distribution was proposed by Betsch and Stein [4], see also Bischoff and Ramm [6]. The strains $E_{\zeta\zeta}$ are evaluated at the element edges and a bilinear strain interpolation in in-plane direction is achieved using bilinear Lagrange shape functions $\bar{N}_i(\xi\eta) = \frac{1}{4}(1+\xi_i\xi)(1+\eta_i\eta)$, which leads to the following equation:

$$\begin{aligned}\tilde{E}_{\zeta\zeta} &= \bar{N}_1(\xi,\eta)E_{\zeta\zeta}(\xi_1=-1,\eta_1=-1) + \bar{N}_2(\xi,\eta)E_{\zeta\zeta}(\xi_2=1,\eta_2=-1) + \\ &\quad \bar{N}_3(\xi,\eta)E_{\zeta\zeta}(\xi_3=1,\eta_3=1) + \bar{N}_4(\xi,\eta)E_{\zeta\zeta}(\xi_4=-1,\eta_4=1)\end{aligned} \tag{7}$$

A closer look shows that the identical strain distribution can be achieved applying the DSG-method for the thickness normal strains $E_{\zeta\zeta}$.

$$E_{\zeta\zeta}^{DSG} = \sum_{i=1}^{n_{np}} N_{,\zeta}^{i} \int_{\zeta_0}^{\zeta_i} E_{\zeta\zeta} d\zeta \tag{8}$$

3.1.6 Nomenclature

In order to simplify the distinction of the used bilinear elements the nomenclature given in Table 1 is introduced. The structure of the notation is 'xxx3Dyyy', where 'xxx' represents the in-plane approximation and 'yyy' the thickness approximation. The numbers in brackets refer to the equations used for the interpolation.

3.2 Biquadratic solid-shell elements

The only biquadratic solid-shell element used in the benchmark study is the 'MI9k3DEAS-at' - element which uses the modifications described in the following subsections. For a more

Elementname	in-plane approximation	thickness approximation
ANS3DEAS	(2)	(6)
DSG3DEAS	(3)	(6)
ANS3DEAS-at	(2)	(6) and (7)
DSG3DEAS-ds	(3)	(6) and (8)
dsg3DEAS-ds	(3) and (5)	(6) and (8)
EAS3DEAS-at	(2) and (4)	(6) and (7)

Tab. 1 Nomenclature of bilinear elements - modified to remove locking

detailed description we refer to [14, 15]. The major expectation is to capture curved geometries in a better fashion than with bilinear interpolation.

3.2.1 Transverse shear and membrane locking

To suppress transverse shear and membrane locking the assumed natural strain method as proposed by Bucalem and Bathe [8] is employed. The assumed membrane strains

$$\begin{aligned} \bar{E}_{\xi\xi} &= \sum_{i=1}^{3}\sum_{j=1}^{2} Q_i^q(\eta) Q_j^l(\xi) E_{\xi\xi}(\xi_j, \eta_i) \\ \bar{E}_{\eta\eta} &= \sum_{i=1}^{3}\sum_{j=1}^{2} Q_i^q(\xi) Q_j^l(\eta) E_{\eta\eta}(\xi_i, \eta_j) \\ \bar{E}_{\xi\eta} &= \sum_{i=1}^{2}\sum_{j=1}^{2} Q_i^l(\xi) Q_j^l(\eta) E_{\xi\eta}(\xi_i, \eta_j) \end{aligned} \tag{9}$$

and the assumed transverse shear strains

$$\begin{aligned} \bar{E}_{\eta\zeta} &= \sum_{i=1}^{3}\sum_{j=1}^{2} Q_i^q(\xi) Q_j^l(\eta) E_{\eta\zeta}(\xi_i, \eta_j) \\ \bar{E}_{\xi\zeta} &= \sum_{i=1}^{3}\sum_{j=1}^{2} Q_i^q(\eta) Q_j^l(\xi) E_{\xi\zeta}(\xi_j, \eta_i) \end{aligned} \tag{10}$$

result from the interpolation

$$\begin{aligned} Q_1^q(z) &= \frac{1}{2}\sqrt{\frac{5}{3}}z\left(\sqrt{\frac{5}{3}}z + 1\right) \\ Q_2^q(z) &= 1 - \frac{5}{3}z^2 \\ Q_3^q(z) &= \frac{1}{2}\sqrt{\frac{5}{3}}z\left(\sqrt{\frac{5}{3}}z - 1\right) \end{aligned} \qquad \begin{aligned} Q_1^l(z) &= \frac{1}{2}(1 + \sqrt{3}z) \\ Q_1^l(z) &= \frac{1}{2}(1 - \sqrt{3}z) \\ z &= \xi, \eta. \end{aligned}$$

The evaluation points for the strain interpolation are depicted in figure 5.

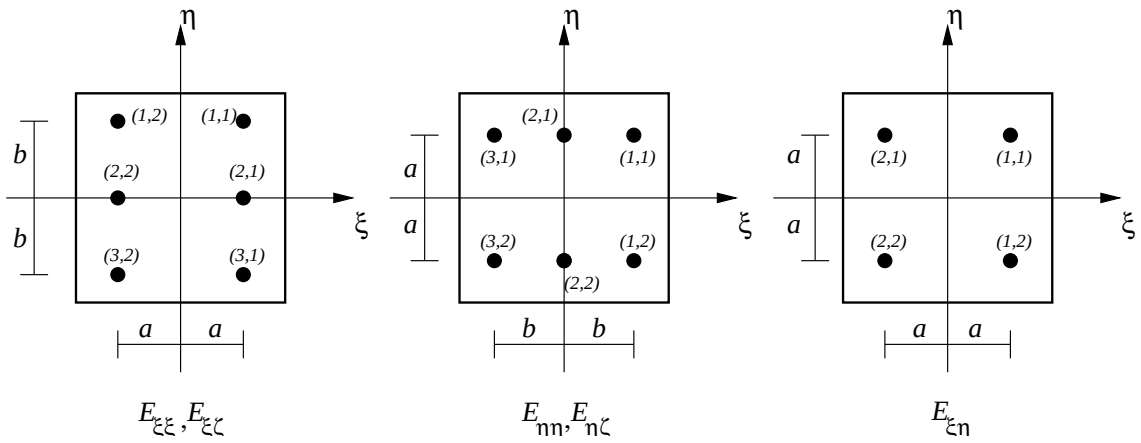

Fig. 5 Evaluation points for strain interpolation, $a = \sqrt{\frac{1}{3}}$, $b = \sqrt{\frac{3}{5}}$

3.2.2 Thickness locking

The phenomenon of thickness locking has already been described for the bilinear solid-shell elements. As for the bilinear elements thickness locking is removed by enhancing the thickness normal strains by use of the EAS method as proposed by Büchter and Ramm [9]. Here 9 additional element parameters α_i are necessary:

$$E_{\zeta\zeta}^{EAS} = E_{\zeta\zeta}^{c} + \frac{1}{det\boldsymbol{J}}\zeta t_{33}^2[1\ \xi\ \eta\ \xi\eta\ \xi^2\ \eta^2\ \xi^2\eta\ \xi\eta^2\ \xi^2\eta^2] \begin{pmatrix} \alpha_1 \\ \vdots \\ \alpha_9 \end{pmatrix} \tag{11}$$

The factor

$$t_{33} = \boldsymbol{G}_3(\xi,\eta,\zeta) \cdot \boldsymbol{G}^3(0,0,0)$$

is needed for the transformation of the enhanced strains to the covariant coordinate system at the element mid-point.

3.2.3 Curvature-thickness-locking

An assumed strain interpolation for the transversal normal strains is used for removing curvature-thickness-locking. Therefore biquadratic Lagrange functions

$$\begin{aligned} \bar{N}_i(\xi,\eta) = & \left(\frac{1}{2}\xi\xi_i(1+\xi\xi_i) + (1-\xi^2)(1-\xi_i^2)\right) \\ & \left(\frac{1}{2}\eta\eta_i(1+\eta\eta_i) + (1-\eta^2)(1-\eta_i^2)\right) \end{aligned}$$

are taken as follows:

$$\begin{aligned} \bar{E}_{\zeta\zeta} = & \bar{N}_1 E_{\zeta\zeta}(\xi_1=-1,\eta_1=-1) + \bar{N}_2 E_{\zeta\zeta}(\xi_2=1,\eta_2=-1) + \bar{N}_3 E_{\zeta\zeta}(\xi_3=1,\eta_3=1) \\ & \bar{N}_4 E_{\zeta\zeta}(\xi_4=-1,\eta_4=1) + \bar{N}_5 E_{\zeta\zeta}(\xi_5=0,\eta_5=-1) + \bar{N}_6 E_{\zeta\zeta}(\xi_6=1,\eta_6=0) \\ & \bar{N}_7 E_{\zeta\zeta}(\xi_7=0,\eta_7=1) + \bar{N}_8 E_{\zeta\zeta}(\xi_8=-1,\eta_8=0) + \bar{N}_9 E_{\zeta\zeta}(\xi_9=0,\eta_9=0). \end{aligned} \tag{12}$$

3.3 Higher order elements (p-FEM)

The results for the higher order elements were provided by the group of Rank and Düster [11, 24]. A p-version FEM based on a hexahedral element was applied to discretize the weak form of the three-dimensional equations of linear elasticity. Therefore, a hierarchic family of high order solid finite elements with an anisotropic Ansatz was constructed. The thin-walled structure situation was taken into account by choosing an appropriate polynomial degree for the three displacement components in the three (local) directions. Due to the hierarchic concept only one finite element implementation is needed and a whole family of different elements can be obtained by simply defining a so-called polynomial degree template [11]. Since the element size is not reduced as the polynomial degree is increased, the description of the geometry has to be independent of the number of elements. Therefore the blending function method was applied to accurately discretize the geometry of the problem [11, 28].

Two different methods for the definition of a polynomial degree template were used. The case in which all elements have the same polynomial degree for all (local) directions and all displacement components is denoted as *isotropic discretization*. The polynomial degree for the displacement components was successively increased $p = 1, ..., 14$. The *anisotropic discretization* refers to the situation where for all elements and all displacement components the polynomial degree q in thickness direction is chosen separately from the in-plane polynomial degree p. In the anisotropic case the polynomial degree in thickness direction is limited to $q \leq 4$. For more detailed information about implementation and application of high order elements for shell problems we refer to [11, 24].

3.4 Benchmark problem

In order to test the different element modifications the cantilever shell depicted in figure 6 is introduced as a benchmark problem originally proposed by Andelfinger [1]. Due to the applied loading the problem is bending dominated. A specific focus is on the positioning of elements with edges not aligned to the generatrix of the shell.

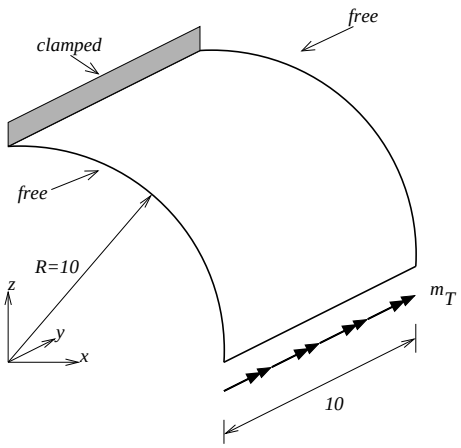

Fig. 6 Benchmark problem: Cylindrical cantilever shell under edge moment loading

The following strategy was chosen for the generation of meshes for the study. First the problem was computed with standard bilinear degenerated shell elements applying different mesh refine-

ment schemes. Three series of meshes where generated starting with the initial discretizations depicted in figure 7 by

1. uniform refinement of the regular initial mesh,
2. adaptive refinement of the regular initial mesh and
3. adaptive refinement of the deliberately distorted initial mesh.

a) regular initial discretization b) distorted initial discretization

Fig. 7 Cylindrical cantilever shell: Initial spatial discretizations for generation of mesh series

Then the problem was computed again with the above described solid-shell elements using the same meshes resp. locations of the nodes. For the biquadratic solid-shell elements further nodes were introduced at the element edges and in the middle of the elements. These nodes were then projected onto the exact curved geometry of the shell as depicted in figure 8 .

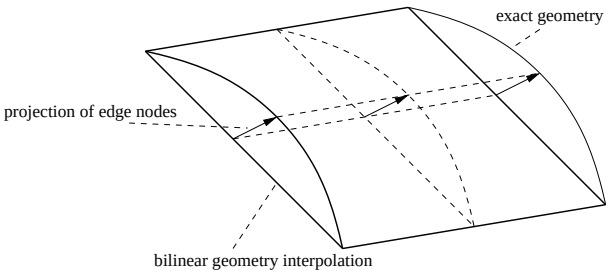

Fig. 8 Projection of additional nodes of biquadratic elements onto exact curved geometry

The reference solution was computed with 121 high order solid elements (p-FEM) applying an isotropic discretization with a polynomial degree $p = 9$. The geometry of the elements was described by combining the blending function method with a polynomial interpolation of geometry, using optimal collocation points [20, 28]. In figure 9 the hexahedral mesh with one element in thickness direction is depicted.

3.5 Results

In the following the results for different element types and different strain modifications are given. For a better comparison the relative errors in the global energy norm of the solutions are depicted in convergence diagrams.

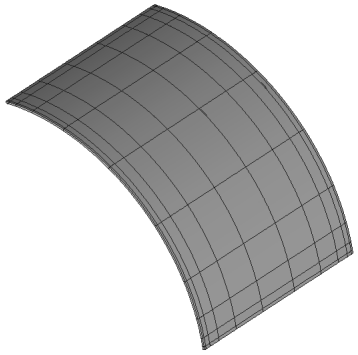

Fig. 9 Cylindrical cantilever shell: Spatial discretization for reference solution with p-elements

3.5.1 Bilinear solid-shell elements - modifications of transversal normal strains

In figure 10 the comparison of the relative errors for the bilinear solid-shell elements with and without modification of the transversal normal strain removing curvature-thickness-locking is shown.

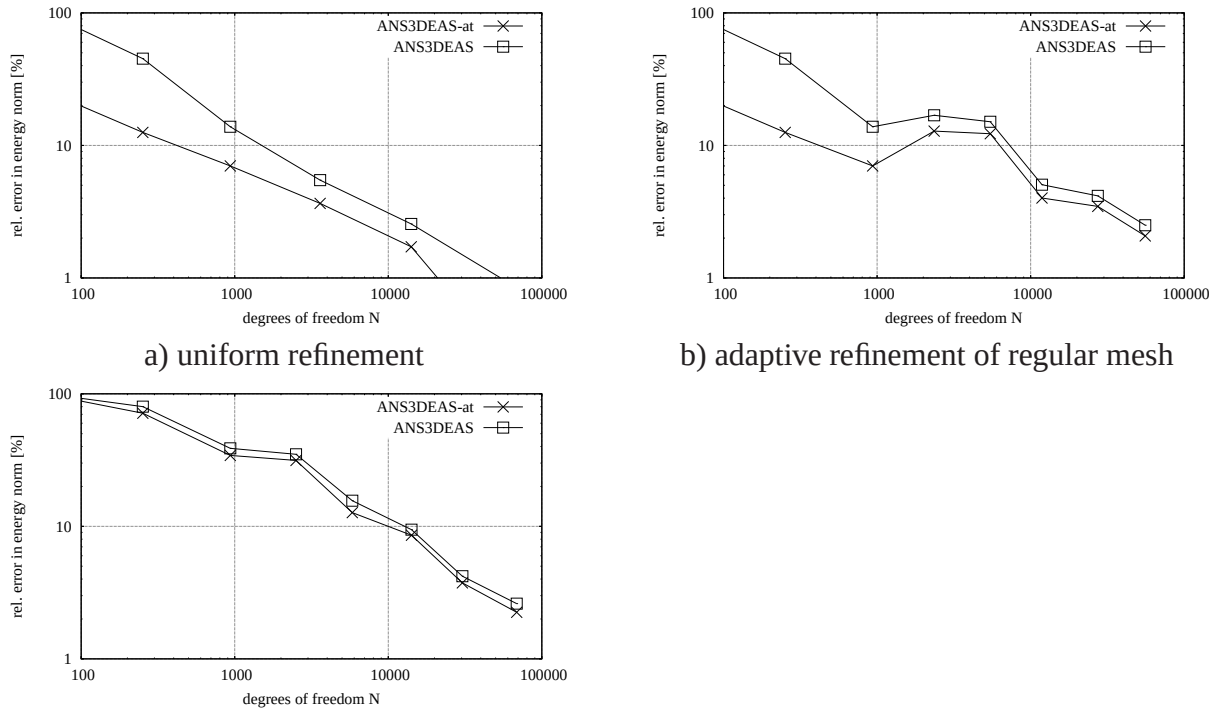

a) uniform refinement

b) adaptive refinement of regular mesh

c) adaptive refinement of distorted mesh

Fig. 10 Cylindrical cantilever shell, computations with different refinement strategies, modifications of transversal normal strains: ANS3DEAS vs. ANS3DEAS-at

Obviously the modified element is superior to the element without modification in the case of the uniform refinement of the regular initial discretization, especially for coarser meshes. This could have been expected since the modification of the transversal normal strains has been tailored for this kind of regular discretization (see figure 4) where all directors point to the local center of curvature of the exact geometry. The transition elements which occur in case of adaptive refinement of the regular mesh strongly perturb this positive effect of the modification.

This is to some extend caused by the fact that here the director of each node is computed via averaging of the directors of the adjacent elements and therefore is not necessarily perpendicular to the exact shell geometry. In case of the disturbed initial discretization the difference in the performance of the two elements nearly vanishes, i.e. the at-modification does not affect the sensitivity of the element to mesh distortions.

3.5.2 Bilinear solid-shell elements - modifications of membrane strains

In figure 11 the results for the EAS and DSG modification of the membrane strains are given comparing the elements for uniform and adaptive refinement of the initially regular mesh.

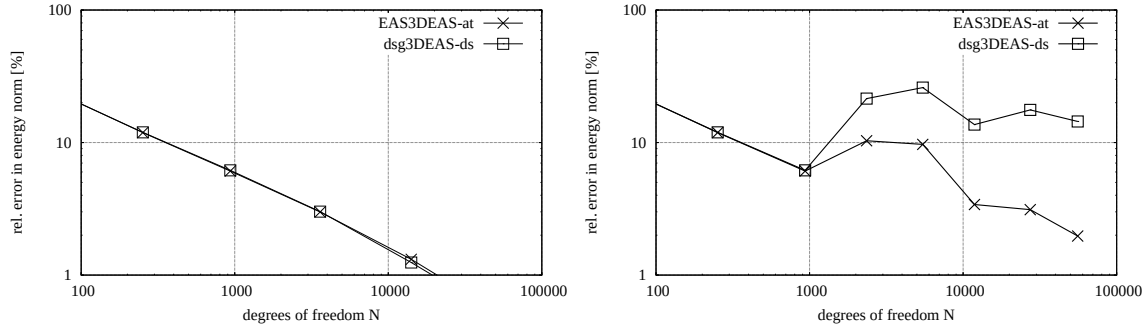

a) uniform refinement b) adaptive refinement of regular mesh

Fig. 11 Cylindrical cantilever shell, computations with different refinement strategies, modification of membrane strains: EAS3DEAS-at vs. dsg3DEAS-ds

Since in this problem no significant membrane locking occurs the modification of the membrane strains is not needed. Thus, there should be no difference in the performance of the elements. In this case the benchmark problem is only suited to check if the modifications have any effect on the distortion sensitivity of the elements. Obviously there is hardly any difference between the results of the EAS and DSG approach in case of the uniform refinement of the regular mesh. However, the diagram for the adaptive refinement of the regular mesh shows that the currently implemented discrete-strain-gap approach seems to be more sensitive to distortions of the mesh than the enhanced strain modification. As a result the modified element performs even worse than the non-modified elements (e.g. ANS3DEAS see figure 10).

3.5.3 Biquadratic solid-shell elements - MI9K3DEAS-at

Figure 12 shows the convergence diagrams of the biquadratic solid-shell element MI9K3DEAS-at. All additional nodes at the edges and in the middle of the elements are located on the exact curved geometry of the shell.

The best results are achieved with the adaptive refinement of the regular mesh. In contrast to the computations with bilinear elements the introduced transition elements have no negative effect on the convergence rate. Therefore in this case the spatially adaptive scheme is superior to the uniform refinement scheme. Even the adaptive refinement of the distorted initial mesh yields results comparable to the uniform refinement of the regular mesh. This is a clear indicator that

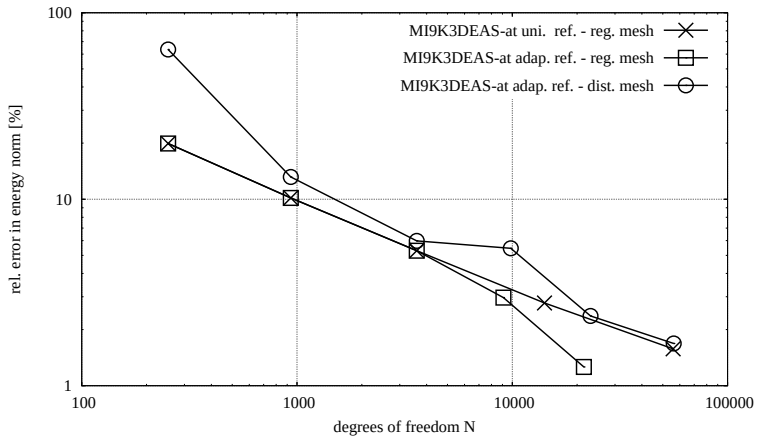

Fig. 12 Biquadratic solid-shell elements - MI9k3DEAS-at

the quadratic interpolation is very important. It remains to be investigated whether this is a result of the geometry or the displacement interpolation.

3.5.4 Biquadratic vs. bilinear solid-shell elements

In figure 13 the comparison of the biquadratic element MI9k3DEAS-at and the bilinear element DSG3DEAS-ds is given.

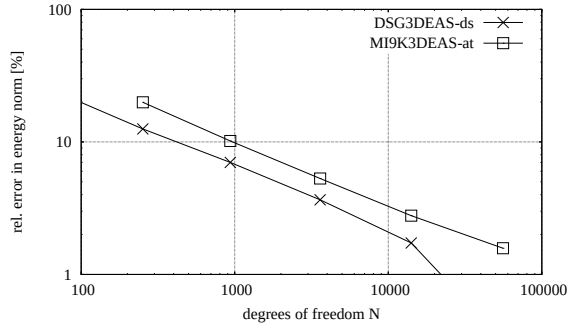

a) uniform refinement

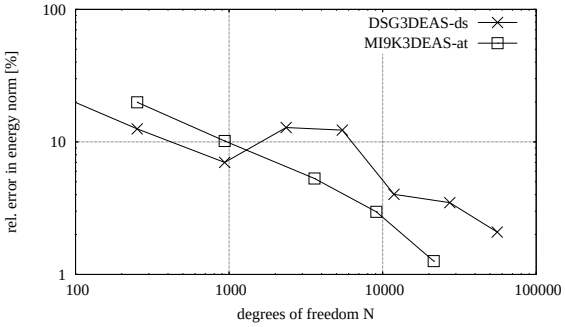

b) adaptive refinement of regular mesh

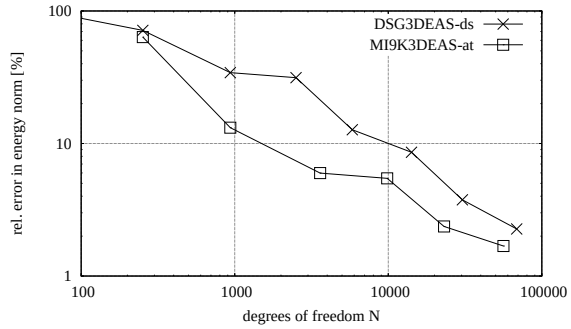

c) adaptive refinement of distorted mesh

Fig. 13 Cylindrical cantilever shell, computations with different refinement strategies, bi-quadratic vs. bilinear solid-shell elements: DSG3DEAS-ds vs. MI9K3DEAS-at

It is interesting to note that the bilinear element is clearly more efficient for the chosen benchmark problem in case of regular meshes. This results from the fact that the chosen benchmark problem results in a nearly constant stress distribution which can be well captured with a linear displacement interpolation.

The only advantage of the biquadratic elements in the given example is the fact that they are less sensitive to mesh distortions than bilinear elements. Therefore the biquadratic element is superior in case of irregular spatial discretizations which result from the adaptive refinement of the regular and distorted initial discretization.

In this context one could presume that the minor sensitivity of the biquadratic elements results from their higher order geometry interpolation which is investigated in the next subsection.

3.5.5 Biquadratic vs. bilinear interpolation of geometry

In order to distinguish if the superior behavior of the biquadratic elements for the given example is a result of the biquadratic map of the geometry a biquadratic interpolation of the geometry is compared to a bilinear interpolation of the geometry.

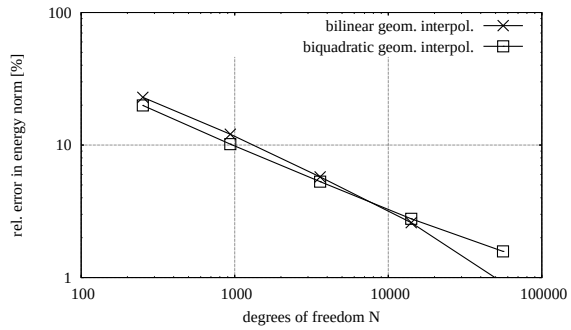

a) uniform refinement

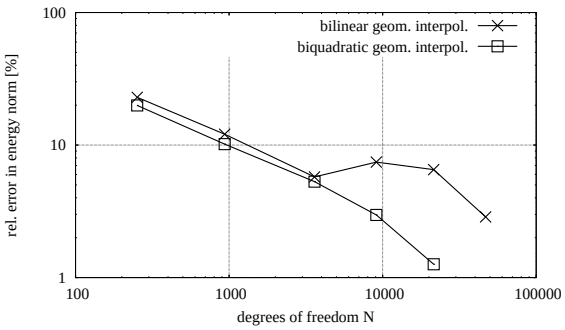

b) adaptive refinement of regular mesh

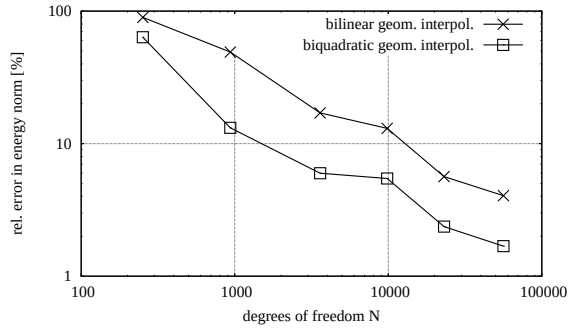

c) adaptive refinement of distorted mesh

Fig. 14 Cylindrical cantilever shell, computations with different refinement strategies, biquadratic vs. bilinear geometry interpolation (MI9K3DEAS-at)

In order to achieve a bilinear geometry interpolation for the biquadratic solid-shell elements the middle nodes of the edges and the center nodes of the nine node element were not projected onto the exact geometry. Thus, the problem is computed with biquadratic displacement interpolation on the geometry of the bilinear elements.

In figure 14 the comparison of the biquadratic and the bilinear interpolation of the geometry is given. Obviously there is hardly any difference in the results in case of the uniform refinement of the regular mesh. But the bilinear map of the geometry results in a stronger sensitivity to mesh distortions which has already been observed for the bilinear elements in the preceding diagrams. Therefore we can conclude that the main source of the sensitivity of the bilinear elements is a result of the bilinear map of the geometry.

3.5.6 p-Elements - isotropic discretization

In figure 16 the results of the p-version based on an isotropic discretization with $p = 1, ..., 14$ are plotted. The initial meshes of the h-adaptive schemes with 9 elements shown in figure 7 were applied also for the p-version, see figure 15, in order to be able to compare the h- and p-version FEM. In the case of the p-version, the geometry of the elements was described with the blending function method, based on a polynomial interpolation of degree $p = 8$, applying optimal collocation points [20, 28].

a) regular mesh b) distorted mesh

Fig. 15 Cylindrical cantilever shell: finite element meshes with 9 high order solid elements

It should be mentioned that with the initial finite element meshes created for the low order elements, boundary layers can not be captured properly and therefore the convergence rate of the p-extension is reduced. To fully exploit the advantages of high order finite elements, proper mesh design - resolving boundary layers and singularities - should be combined with an increase of polynomial degree [11, 24, 28].

The results presented in figure 16 show that high order elements are less prone to distortion, since for $p \geq 5$ no significant difference between the regular and distorted finite element mesh can be observed. Furthermore it is evident that locking effects are removed, as the polynomial degree is increased.

3.5.7 p-Elements - anisotropic discretization

In figure 17 the results obtained with anisotropic high order solid elements are depicted. The in-plane polynomial degree $p = 1, ..., 14$ is successively increased while the polynomial degree in thickness direction q is kept constant at either $1, 2, 3$ or 4. The computations are based on the distorted mesh as presented in figure 15-b). For comparison the corresponding results of the biquadratic MI9k3DEAS-at element and the isotropic discretization based on the p-version are also plotted in figure 17.

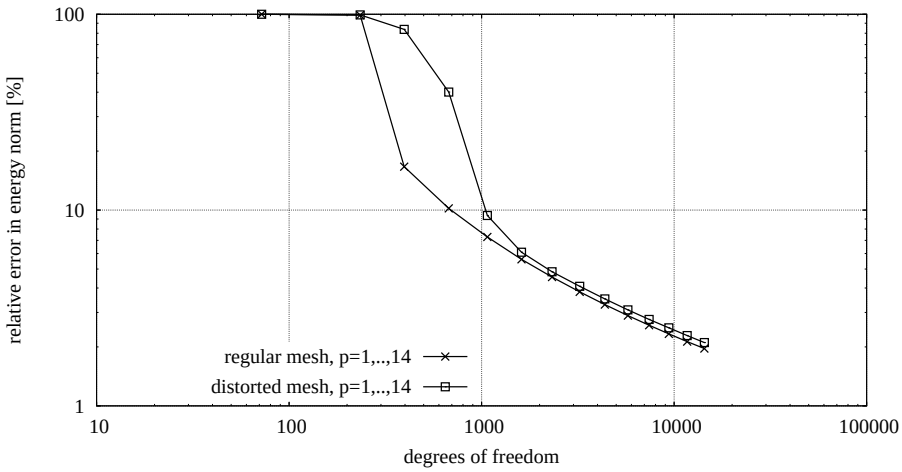

Fig. 16 Cylindrical cantilever shell, p-FEM: isotropic discretization

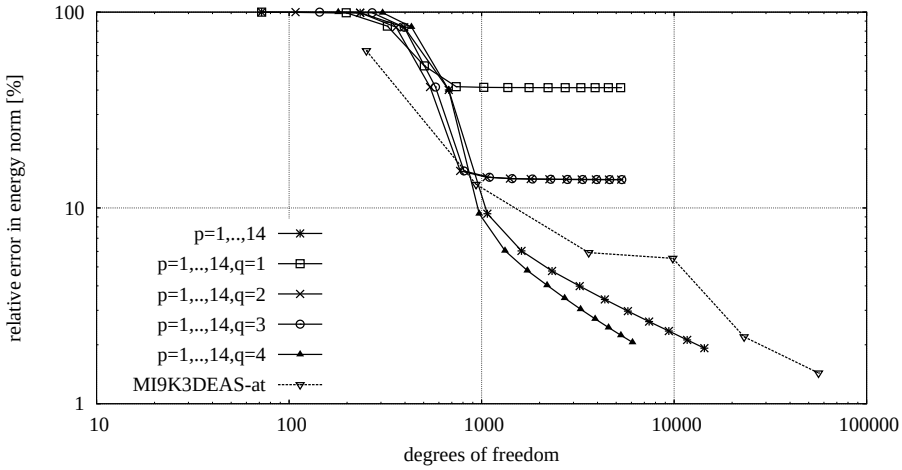

Fig. 17 Cylindrical cantilever shell, p-FEM: isotropic and anisotropic discretization, MI9k3DEAS-at added for comparison

Considering the different polynomial degrees q in thickness direction it can be observed that for $q \leq 3$ the relative error in energy norm does not decrease further as the in-plane polynomial degree p is increased. This is due to the fact that the choice of the polynomial degree q in thickness direction can be interpreted as a model assumption. Therefore, selecting $q \leq 3$ corresponds to accepting a certain model error. However, if we choose $q = 4$ the model error (with respect to the fully three-dimensional solution) is strongly reduced. As expected the anisotropic discretization with $q = 4$ is more efficient than the isotropic discretization since it accounts for the fact that a shell is a thin-walled structure which claims for a higher order interpolation in in-plane direction than in thickness direction.

It is interesting to note that - for this particular mesh - the results for the biquadratic solid-shell element are comparatively well and that the applied modifications of the strains in thickness directions are sufficient to obtain an approximation with an accuracy not being dominated by the model error.

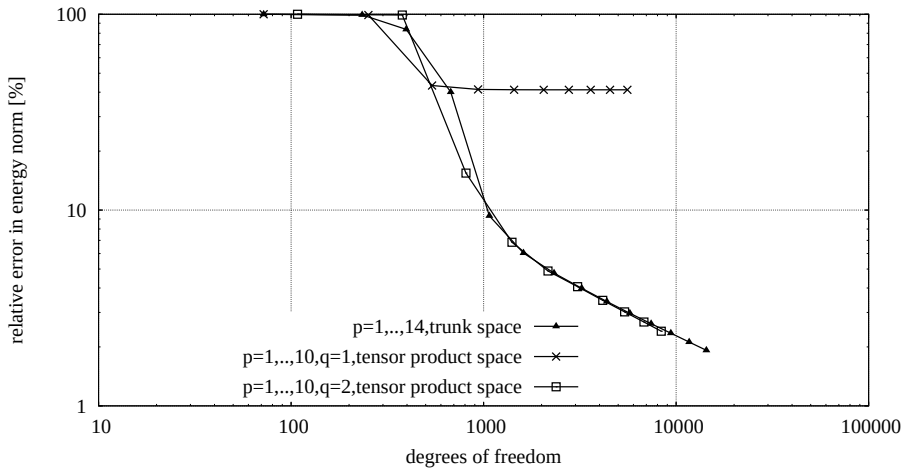

Fig. 18 Cylindrical cantilever shell, p-FEM: anisotropic discretization based on the tensor product space, isotropic trunk space added for comparison

It might be surprising that a polynomial degree in thickness direction as high as $q = 4$ is needed in order to obtain an approximation which is not dominated by the model error. This relatively high polynomial degree q is due to the fact that the results of the p-extension presented in this paper are based on the trunk space. In [11, 24, 28] three different trial spaces have been compared, the trunk space, the tensor product space and the anisotropic tensor product space. The main difference between the three trial spaces is the number of shape functions which are provided for a given polynomial degree. The trunk space provides the lowest number of shape functions while the tensor product space yields the highest number of shape functions.

In figure 18 the results obtained with the tensor product space with $q = 1$ and $q = 2$ are plotted. For comparison, the results of the isotropic discretization based on the trunk space are also displayed. Applying the tensor product space to the computation of the cylindrical cantilever shell one finds that a polynomial degree in thickness direction of $q = 2$ is sufficient to obtain an approximation which is not dominated by the model error. This can be explained by the fact that for $q = 2$ the tensor product space offers shape functions which are not yet present in the trunk space, i.e. are introduced in the trunk space for higher polynomial degrees. Although the application of the trunk space calls for slightly higher polynomial degrees, detailed numerical studies have demonstrated that the trunk space in combination with an anisotropic Ansatz provides the most efficient discretizations. For further information the reader is referred to [11, 24, 28].

4 Conclusions

The study deals with the comparison of different - so-called mixed - modifications of bilinear and biquadratic solid-shell elements and higher order p-elements in a bending dominated numerical example. In order to generate irregular spatial discretizations for the solid-shell elements a hierarchical adaptive mesh refinement scheme was applied. Interestingly all modifications for the low order - in particular the bilinear - elements only work well for regular discretizations capturing the curvature of the shell well. In case of distorted meshes most of the

modifications do not affect and thus not improve the solution behavior in this bending dominated problem. The results of the biquadratic elements show that a biquadratic map of the geometry reduces the sensitivity of the elements improved with mixed modifications to mesh distortions and therefore results in a more robust scheme. The biquadratic element MI9k3DEAS-at leads to good results even compared to the p-version of the finite element method which - as expected - yields the best convergence rates. It should be noted that all the conclusions drawn here are in most instances restricted to the chosen benchmark problem and can not yet be generalized to all types of problems.

References

[1] Andelfinger, U. *Untersuchungen zur Zuverlässigkeit hybrid-gemischter Finiter Elemente für Flächentragwerke*, Dissertation, Universität Stuttgart, 1991

[2] Bathe, K.-J.; Iosilevich, A.; Chapelle, D. *An evaluation of the MITC shell elements*, Computers and Structures, 75:1–30, 2000

[3] Baumann, M. *Lineare Finite Element Konzepte für Schalentragwerke unter Berücksichtigung von adaptiven Methoden*. Dissertation, Institut für Baustatik, Universität Karlsruhe, 1994

[4] Betsch, P. and Stein, E. *An assumed strain approach avoiding artificial thickness straining for a non-linear 4-node shell element*, Communications in Numerical Methods in Engineering, 11:899–909, 1995

[5] Bischoff, M.; Koschnick, F.; Bletzinger, K.-U. *Stabilized DSG elements: A new paradigm in Finite Element Technology*, Proc. of the 4.th European LS–DYNA Conference, Ulm,Germany, 2003

[6] Bischoff, M.; Ramm, E. *Shear deformable shell elements for large strains and rotations*, Int. J. Numer. Methods Eng., 40:4427–4449, 1997

[7] Bletzinger, K.-U.; Bischoff, M.; Ramm, E. *A unified approach for shear-locking-free triangular and rectangular shell finite elements*, Computers and Structures, 75:321–334, 2000

[8] Bucalem, B.N; Bathe, K.J.. *Higher order MITC general shell elements*, Int. J. Numer. Methods Eng., 36:3729–3754, 1993

[9] Büchter, N.;Ramm, E. *3D-Extension of Nonlinear Shell Equations Based on the Enhanced Assumed Strain Concept*, Computer Methods in Applied Sciences, 55–62, 1992

[10] Büchter, N.; Ramm, E.; Roehl, D. *Three Dimensional Extension of Nonlinear Shell Formulation Based on the Enhanced Assumed Strain Concept*, Int. J. Numer. Methods Eng., 37:2551–2568, 1994

[11] Düster,A.; Bröker, H.; Rank,E. *The p-version of the Finite Element Method for three-dimensional curved thin walled structures*, Int. J. Numer. Methods Eng., 52:673–703, 2001

[12] Dvorkin, E.; Bathe, K.J. *A continuum mechanics based four-node shell element for general nonlinear analysis*, Engineering computations, 1:77–88, 1984

[13] Gebhardt, H. *Finite Element Konzepte für schubelastische Schalen mit endlichen Drehungen*, Dissertation, Institut für Baustatik, Universität Karlsruhe, 1990

[14] Harnau, M. *Finite Volumen–Schalenelemente für große Deformationen und Kontakt*, Dissertation, Universität Karlsruhe, 2004

[15] Harnau, M.; Schweizerhof, K. *About linear and quadratic "solid-shell" elements at large deformations*, Computers and Structures, 80:805–817, 2002

[16] Hauptmann, R. *Strukturangepaßte geometrisch nichtlineare Finite–Elemente–für Flächentragwerke*, Dissertation, Universität Karlsruhe, 1997

[17] Hauptmann, R.; Doll, S.; Harnau, M.; Schweizerhof, K. *Solid-Shell Elements with Linear and Quadratic Shape Functions at Large Deformations with Nearly Incompressible Materials*, Computers and Structures, 79:1671–1685, 2001

[18] Hauptmann, R.; Schweizerhof, K. *A systematic development of 'solid-shell' element formulations for linear and non-linear analyses employing only displacement degrees of freedom*, Int. J. Numer. Methods Eng., 41:00–01, 1998

[19] Havu, V.; Pitkäranta, J. *Analysis of a bilinear finite element for shallow shells I: Approximations of inextensional deformations*, Technical report, Helsinki University of Technology, 2000

[20] Királyfalvi,G.; Szabó,B.A. *Quasi-regional mapping for the p-version of the finite element method*, Finite Elem. Anal. Des. , 27:85–97, 1997

[21] Koschnick, F. *Geometrische Locking-Effekte bei Finiten Elementen und ein allgemeines Konzept zu ihrer Vermeidung*. Dissertation, Technische Universität München, 2004

[22] Lee, P.-S.; Bathe, K.-J. *On the asymptotic behavior of shell structures and the evaluation in finite element solutions*, Computers and Structures, 80:235–255, 2002

[23] Pitkäranta,J.; Leino,Y.; Ovaskainen,O.; Piila, J.. *Shell deformation states and the finite element method: A benchmark study of cylindrical shells*, Comput. Meth. Appl. Mech. Eng., 128:81–121, 1995

[24] Rank, E.; Düster, A.; Nübel, V.; Preusch,K.; Bruhns,O.T. *High order finite elements for shells*, Comput. Meth. Appl. Mech. Eng., 194:2494–2512, 2005

[25] Riccius, J.; Schweizerhof, K.; Baumann, M. *Combination of adaptivity and mesh smoothing for the Finite Element analysis of shells with intersections*, Int. J. Numer. Methods Eng., 40:2459–2474, 1997

[26] Simo, J.C.; Rifai, M.Si. *Geometrically non-linear enhanced strain mixed methods and the method of incompatible modes*, Int. J. Numer. Methods Eng., 33:1413–1449, 1990

[27] Simo, J.C.; Armero, F. *Geometrically non-linear enhanced strain mixed methods and the method of incompatible modes*, Int. J. Numer. Methods Eng., 33:1413–1449, 1992

[28] Szabó, B.A., Düster,A.; Rank, E. *The p-version of the finite element method*, Encyclopedia of Computational Mechanics, E. Stein, R. de Borst, T.J.R Hughes (eds), vol. 1:119-139, Wiley, 2004

[29] Zienkiewicz, O.C.; J.Z. Zhu, J.Z. *The superconvergent patch recovery and a posteriori error estimates. part 1: The recovery technique*, Int. J. Numer. Methods Eng., 33:1131–1364, 1992

[30] Zienkiewicz, O.C.; J.Z. Zhu, J.Z. *The superconvergent patch recovery and a posteriori error estimates. part 2: Error estimates and adaptivity*, Int. J. Numer. Methods Eng., 33:1365–1382, 1992